Effect of lanthanum doping on structural, optical, and photocatalytic properties of YVO4

Erkul Karacaoglu (ekaracaoglu@kmu.edu.tr)
Karamanoglu Mehmetbey University
Ozlem Altintas Yildirim
Konya Technical University
Teoman Ozturk
Selcuk University
Mert Gul
Eskisehir Technical University

Research Article

Keywords: Solid state reaction method, YVO4, La3+ doped YVO4, photocatalytic, RhB, photoluminescence

Posted Date: January 10th, 2023

DOI: https://doi.org/10.21203/rs.3.rs-2446037/v1

Abstract

Yttrium vanadate (YVO_4) based undoped and La^{3+}-doped powders were prepared through a solid-state reaction method. The structural characterization carried out with XRD indicating that the samples are crystalline tetragonal type crystal structure of YVO_4. XRD of the YVO_4: La^{3+} powder contain same YVO_4 diffraction lines and no other lanthanum related impurity and/or secondary phases were detected. Both undoped and La^{3+}-doped YVO_4 samples show combined white light emission peaks appeared at 478, 571 and 613 nm. The higher intensity of peaks located at 478 and 571 nm in YVO_4: La^{3+} sample can be attributed to O^{2-}-La^{3+} and O^{2-}-V^{5+} charge transfer mechanisms. Besides, photocatalytic activities of the undoped and La^{3+} doped YVO_4 samples were investigated under the UV light irradiation monitoring the aqueous solution of methylene blue (MB) dye. Hence, the effects of La^{3+} dopant ion on the photoluminescence properties are discussed in detail. While the degradation of MB reaches to 38.8% after 180 minutes of UV light exposure with undoped YVO_4, the degradation efficiency of La^{3+} doped YVO_4 reaches 76.7%. Pseudo-first-order reaction rate constant (k) of La^{3+}-doped YVO_4 (0.00846 min^{-1}) is determined 66% greater than undoped one (0.00287 min^{-1}).

1. Introduction

Water pollution due to industrialization and increasing need for fresh water with rapid population growth have become a major environmental problem worldwide. Moreover, another harsh truth is that only 2.5% of the total water volume in the world is fresh water [1]. Furthermore, the covid 19 pandemic has made clear that water purification, hygiene and wastewater treatment are not only beneficial to the environment but also to human health. Semiconductor photocatalysts have been used extensively as remediation materials for the degradation of dye-related pollutants in water. Since the pioneering study of Fujishima and Honda, a tremendous effort has been endeavored to the development of novel heterogeneous semiconductor photocatalysts for the degradation of pollutants [2]. Recently, orthovanadates such as, $InVO_4$, $BiVO_4$, $MnVO_4$ and YVO_4, etc. have been also used as efficient photocatalysts in photocatalytic degradation applications [3–7]. Among the orthovanadates, YVO_4 has a wide band gap energy (3.38 eV) and can be excited by UV light. Although the use of only UV irradiation is considered a disadvantage in terms of photocatalysis, the wide band gap of YVO_4 allows the excited electrons and holes to exhibit a strong redox capability [8]. Besides, YVO_4 nanostructures exhibit high thermal, mechanical and chemical stability and have a strong birefringence which is well convenient for many optical applications [9, 10].

In one of the first studies on the photocatalytic of YVO_4, Xu et al. synthesized YVO_4 nanopowders via microwave irradiation and investigated their photocatalytic properties via decolorization of methyl orange [11]. Liu et al. prepared YVO_4 nanoparticles via molten salt method at a low temperature and their photocatalytic activity was investigated by the degradation of rhodamine B (RhB) [12]. Yang et al. produced YVO_4 nanoparticles at room temperature by a direct precipitation method which provide to control the crystallinity and concentration of oxygen vacancies, so provide to enhance in the

photocatalytic efficiency of YVO_4 nanoparticles [13]. Sized-controlled YVO_4 nanoparticles were also produced via hydrothermal method and performed photocatalytic measurements through the degradation of methylene blue [14]. In an interesting study, YVO_4 powders produced by the combustion and hydrothermal method were used in RhB dye degradation and embryotoxicity tests of zebrafish and RhB solutions degraded using these powders [15].

YVO_4 finds places in many technological and optical applications owing to their special 4f–5d and 4f–4f electronic transitions. Nd: YVO_4 has been used in laser crystals [16] and diode pumped solid-state lasers [17]. Eu doped YVO_4 powders has been used as the red phosphor in color televisions and cathode ray tubes [18]. In an important paper, Shiraishi et al. investigated the photoluminescence and the photocatalytic activity of different amount of Eu doped YVO_4 nanoparticles via degradation of methyl orange [19]. Also, they obtained the photoluminescence (PL) spectra and proposed these NPs as a model compound of a multimodal photoenergy converter. For comparison, they also investigated La doped YVO_4 NPs. Besides the photoluminescence, upconverting ability of lanthanide doped YVO_4 makes these materials quite remarkable recently. With upconversion nanomaterials (UCNPs), near-infrared light can be converted into visible or ultraviolet light which triggers photoreactions of photosensitive materials [20]. Lanthanide doped YVO_4 UCNPs exhibit UC emission peaks which includes f-d and f-f transitions of lanthanide ions [9, 21].

In this study, undoped and La-doped YVO_4 powder samples were synthesized by solid state reaction method under open atmosphere. Structural, morphological, and optical properties of the phosphors were investigated via x-ray diffraction (XRD), scanning electron microcopy (SEM) / energy dispersive X-ray (EDX) spectroscopy, photoluminescence spectrometer (PL) analyses at room temperature, respectively. The photocatalytic activities of the undoped and La^{3+}-doped YVO_4 powders were determined through the degradation of methylene blue (MB) dye under UV light irradiation. In the photocatalytic performances, it was observed that doping of La has an impressive effect on the photocatalytic activity of YVO_4. Moreover, the possible mechanism involved in the photocatalytic reaction and photoluminescence was proposed in detail.

2. Experimental Procedure

2.1. Materials

Yttrium (III) oxide (Y_2O_3, 99.99%, Aldrich), vanadium (V) oxide (V_2O_5, 99.5%, Stanford Materials), lanthanum (III) oxide (La_2O_3, 99.99%, Merck), and isopropyl alcohol (BioReagent, for molecular biology, ≥ 99.5%) were used as starting materials. Further purification is not needed for these chemicals. High purity alumina crucibles were used throughout the heat treatments. The heat treatments were carried out in a muffle furnace (Nevola Reis 130/45).

2.2. Preparation of samples

Undoped and La^{3+}-doped YVO_4 powder samples were prepared by typical solid state reaction method. The stoichiometric mixtures of starting materials were precisely weighed and well mixed in zirconia bowls using zirconia balls and isopropyl alcohol in planetary mill at 250 rpm for 1 hour. Then the wet mixtures were dried for 24 hours at 100°C. Two step heat treatment process was conducted at 500°C for 4 hours and at 900°C for 4 hours in open atmosphere, respectively. There was no need to grind the powders after the heat treatment. Finally, the characterization and analysis process were carried out.

2.3. Characterization

Phase purity and crystal structures were examined with a RIGAKU Rint 2000 model x-ray diffractometer, which run at 40 kV and 30 mA (Cu-Kα radiation). The particle morphology and size distributions of powders were investigated by Zeiss, SUPRA 50 VP model SEM using an accelerating voltage of 20 kV. PL spectra were recorded on two type of Fluorescence spectrophotometers which are Photon Technology International (PTI), QuantaMaster™ 30 and Hitachi F-7100. Both the PL measurement devices set with spectral slit width of 5 nm, has a Xe lamp as the excitation source and were carried out at room temperature. The optical absorption spectra properties of the samples were measured with a Shimadzu UV-1800 UV/Visible scanning spectrophotometer.

2.4. Evaluation of photocatalytic activity

Photocatalytic activities of the undoped and La^{3+}-doped YVO_4 powder were evaluated by monitoring the degradation of MB under the UV light irradiation. In the experiments 6 Osram UV-C lamps with 8 watts were used as the sources of UV light. The photocatalytic activities of the powders were evaluated using a Cary 5000 UV–Vis spectrophotometer. All measurements were carried out at room temperature and aqueous MB dye solution prepared at a concentration of 5 ppm was used as the model of pollutant. After adding 50 mg of powders into the MB solution, it was firstly stirred for 60 minutes in the dark for adsorption-desorption equilibration. Then, photocatalytic activities were evaluated by absorbance measurements of 3 ml of MB dye solution collected at 15 min intervals.

3. Results And Discussions

3.1. Structural analysis

To investigate the effect of La addition on the crystal structure of YVO_4, XRD analyses of the undoped YVO_4 and La^{3+}-doped YVO_4 powders have been employed. Figure 1(a) and (b) show XRD diffractograms of samples prepared with solid state reaction method. It was found that all the strong diffraction lines correspond to expected (200), (211), (400), (422), (433) and (600) diffraction reflections of crystalline tetragonal type crystal structure of YVO_4 (JCPDS card no: 17–0341) .The XRD pattern of undoped and the La^{3+}-doped YVO_4 contain same YVO_4 diffraction lines with similar relative intensities and no other diffraction lines related with any lanthanum based compounds like La_2O_3 and $La(OH)_3$, or other impurity phases were detected within the detection limit of the XRD. In the previous studies, thermal equilibrium

solubility limit of La in YVO_4 was found as 6 at.% with coprecipitation method [19]. In this study, the dopant amount of YVO_4 is chosen much lower than the solubility of La in YVO_4. Therefore, according to XRD results, substitutional incorporation of the La^{3+} ions into YVO_4 crystal is expected for the studied dopant concentration.

In order to obtain detailed structural information, the crystallite size (D, in nm) of the powders were calculated by Scherrer's Eq. (1) using the XRD line broadening method:

$D = 0.9\lambda/\beta\cos\theta$ (1)

where λ is the X-ray wavelength for CuKα, β is the full width in radians half maximum of the diffraction line and θ is the Bragg angle of (211) peak. B is determined by $\beta = (\beta_{obs}^2 - \beta_{ins}^2)$, β_{obs} is the measured broadening and β_{ins} is the instrumental broadening caused by the diffractometer. First, a decrease is observed on crystallite size, D, with La dopant. D value of 45.5 nm and 30.9 nm were obtained at undoped and La^{3+}-doped YVO_4, respectively, which suggest that there can be hindering of the crystal growth by the substitutionally incorporation of La^{3+} ions.

The effect of the La incorporation on the YVO_4 crystal structure can be also investigated by examining the peak intensities and positions of YVO_4 patterns as shown Fig. 1(c). It is found that the relative (211) peak intensities of undoped YVO_4 drastically decreased by La doping which implies that dopant atoms inhibit the crystal growth of YVO_4 particles at preferential growth direction. Furthermore, (211) diffraction line positions of undoped and La doped samples were determined as 2θ=~24.93° and ~ 24.84°, respectively. According to XRD spectra, insignificantly peak shift is observed to relatively lower 2θ values. The lattice parameters (a) and (c) variation is tabulated to observe doping effect. For undoped YVO_4 particles, the lattice constants (a) and (c) are calculated as 7.135 and 6.27 Å, respectively. However, YVO_4: La^{3+} powder demonstrates a slight lattice expansion with calculated lattice parameters (a) = 7.14 Å and (c) = 6.31 Å. The lattice expansion observed in the La^{3+}-doped sample can be attributed to the substitution of La^{3+} ions into the Y^{3+} sites due to larger ionic radius of La^{3+} (1.172 Å) than that of Y^{3+} (1.140 Å) for the same coordination number [22]. It is normal that this expansion (hence the peak shift in the XRD pattern) has been sensitively affected as the doping rates are low. This perturbation on lattice parameters depending on La addition is preliminarily evident that incorporated La ions was selectively substitute into Y^{3+} sites of YVO_4 crystal.

3.2. Morphological and elemental analysis

The SEM photographs (Figs. 2a and 3a) of the undoped and La^{3+}-doped YVO_4 phosphor powders both exhibits partially agglomerated grains and irregular particles both in shape and size. The EDS profile of both phosphor powders (Figs. 2b and 3b) indicate the presence of Yttrium, Vanadium, and Oxygen

elements what in each sample should include. Furthermore, in the EDS profile of La^{3+}-doped YVO_4 powder, addition peaks related with Lanthanum was observed.

3.3. Photoluminescence of undoped and La^{3+}-doped YVO_4

The PL spectra of undoped YVO_4 and YVO_4: La^{3+} powders in Fig. 4a show same excitation peaks and considerable number of emission peaks between 450 and 750 nm, representing the similar positions of peaks by varying intensities. The PL emission spectrum of undoped YVO_4 has two clear peaks in the wavelength range of 600–800 nm (Fig. 4b) which the major peak is at 620 nm. The other peak at 710 nm can be related to the recombination of electrons and holes at oxygen vacancies in YVO_4. The maximum intensity emission peak located at 571 nm for YVO_4: La^{3+} powder may be assigned to singly ionized oxygen vacancies which became dominated after La^{3+} doping. With the La^{3+} doping, emission bands from 450 to 650 nm were greatly suppressed and emission around 571 nm became the dominated component on the emission spectra of YVO_4: La^{3+}. The red luminescence centered at 620 nm was suppressed with respect to the blue one (at 478 nm) and the yellowish green one (at 571 nm) which are also the low intensity bands of undoped YVO_4. This indicates La^{3+} doping modifies intrinsic lattice defects and intensively changes luminescence characteristic with respect to luminescence of undoped YVO_4 [23, 24].

PL excitation and emission spectra given in Fig. 4 depicts the similar luminescence characteristics of undoped and La^{3+} doped YVO_4 powder samples. The reason for red-shift from 282 nm to 290 nm in PL excitation spectra of undoped and La^{3+}-doped YVO_4 powders, respectively can be assigned to the La^{3+} doping, hence O^{2-}-La^{3+} charge transfer (CT) from oxygen 2p excited state to La^{3+} 4f state and O^{2-}-V^{5+} CT from oxygen 2p states to the empty d states of central vanadium in the VO_4^{3-} group, indicating that there is a strong energy migration from host to La^{3+}-activator in tetragonal YVO_4 [25]. Further, the detailed study of PL emission spectrum of undoped YVO_4 powder is shown in Fig. 5. The intense broad emission peak centered at 620 was deconvoluted using Gaussian fitting in the wavelenumber (cm^{-1}) unit of energy to be able to interpret and demonstrate in detail the various defects/vacancies present in the system, as shown in Fig. 5. All these peaks combined with the major peak at 16130 cm^{-1} (620 nm) obtained after deconvolution could be specified to emission as shallow and deep level trap states. Hence, it can be said that oxygen vacancies are the prime defects responsible for PL emission. The emission peak at 485 nm for undoped YVO_4 could correspond to characteristic intrinsic emission of VO_4^{3-} groups [26] defect related luminescence and/or surface impurities such as oxygen vacancies, intrinsic defects and surface state and intrinsic metal ions in YVO_4 crystal formed during growth. Accordingly, the effect of La^{3+} dopant ion has emerged based on the luminescence properties of the undoped material since they have same host crystal. In previous studies with similar results demonstrates doping of impurities with different oxidation state can create or increase defect levels [27, 28]. The impurity ions could give raise to either radiative or non-radiative recombination. In this case and studied material, La ion plays a

significant role in modifying the defect chemistry of YVO_4 which can be clearly seen in the variation in PL intensities between undoped and La doped YVO_4. The effect of La additive on lattice is as follows: Along with doping, La ion migrates inside the YVO_4 lattice and occupies the vacancy site. There could not be charge imbalance and ionic radii mismatch affect because it was supposed to be that La^{3+} ions could substitute the Y^{3+}-sites since ionic radii are close to each other (La^{3+}= 1.172 Å vs Y^{3+}= 1.140 Å). The defects in YVO_4 may also vary with synthesis method and condition, particle size and morphology, hence, the emission peak at 485 nm, which is of relatively low intensity compared to the others is related to deep level defects of La^{3+}-doped YVO_4.

3.4. Absorption spectra of undoped and La^{3+}-doped YVO_4

Figure 6 shows the absorption spectra of undoped and La^{3+} doped YVO_4 powders.

It can be clearly made inference that both the samples are nearly transparent in the visible region between 400–800 nm. La-doped sample being a little more evident and severe, also exhibit an intense band-to-band absorption originated from the contribution of $^1A_1 \rightarrow {}^1T_1$ charge transition around 300 nm overlapped with $^1A_1 \rightarrow {}^1T_2$ charge transition at between 200–350 nm of VO_4^{3-} groups. Additionally, the powder colors formed in both undoped and La^{3+}-activated YVO_4 samples have a light-yellow color, which can be attributed to the reduction of V^{5+} to V^{4+}, subsequently formed V^{4+} defects and oxygen vacancies. It can be concluded that the formation of V^{4+} defects is rather related with redox between Ln^{3+} (here, Ln means La) ions and different types of vanadium ions [26, 29].

Energy band gap (E_g) of the undoped and La doped YVO_4 nanoparticles were obtained using the well-known Tauc plot which is depicted in Fig. 7. Tauc method relies on the following equation:

$$(\alpha h\upsilon)^{1/n} = A\left(E_g - h\upsilon\right)$$

2

Where α is the absorption coefficient, $h\upsilon$ is the energy of the incident photon, A is a constant and n depends on the optical transition of the material. YVO_4 possess a direct transition ($n = 1/2$) and a band gap of 3.8 eV [30]. As given in Fig. 7, E_g of undoped YVO_4 is obtained as 3.8 eV from fit of the red curve which is consistent with the literature. On the other hand, E_g of the YVO_4: La is determined as 3.5 eV from the fit of the blue curve. This decrease in energy band gap with doping is highly desirable for the photocatalytic performances. It is obvious that doping YVO_4 with La will provide an increase in the photocatalytic activity due to formation of new localized energy levels between valence and conduction band.

3.5. Photocatalytic activity of YVO_4 phosphors

To understand the influence of lanthanum dopant on the photoactivity of the YVO_4, the photocatalytic activities of undoped and La^{3+}-doped YVO_4 powders have been evaluated by degradation of MB dye under UV light irradiation. Photocatalytic reaction was carried out with a UV light exposure time of 180 minutes. The wavelength of maximum absorbance of MB at 664 nm was used for the measurement of MB concentration. As seen in Fig. 8, a set of experiments were performed with the photocatalysts and MB under UV light irradiation. Both figures show decreases at the vicinity of 664 nm with a slightly shift. This little hypsochromic shift (blue shift) is attributed to N-demethylation of MB [31].

The normalized temporal concentration changes of photocatalytic degradation of MB aqueous solution in the presence of the photocatalysts were shown in Fig. 9a. As seen in Fig. 9a, La^{3+}-doped YVO_4 with 76.7% degradation efficiency led to more degradation under UV light illumination compared to the undoped one (38.8%). These results show that the photocatalytic activity of YVO_4 changes and enhances with the substitutionally incorporation of La^{3+} ions into YVO_4 crystal structure. The photocatalytic degradation rate of MB dye solutions fits a pseudo-first-order reaction model which is based on the Langmuir-Hinshelwood mechanism and can be calculated from the following equation:

$$-\ln\frac{C_t}{C_0} = k_{app}t$$

3

where C_0 is the initial concentration of the dye, C_t is the concentration at irradiation time t and k_{app} is the apparent pseudo-first-order reaction rate constant. The plots of $-\ln\left(C_t/C_0\right)$ versus time t are given in Fig. 9b for UV irradiation. The k_{app} values were calculated from the slope of these curves. According to the results obtained, the k_{app} values are 0.00287 min^{-1} and 0.00846 min^{-1} for YVO_4 and La^{3+}-doped YVO_4 particles, respectively. This result shows that La doping increases the k_{app} value by 66%.

A possible mechanism can be proposed to explain the increasing in the photocatalytic activity as follows (Fig. 10): YVO_4 can only be excited by UV light (λ < 367 nm) due to its wide band gap (3. 8 eV) [30]. La doping results in localized impurity levels between the conduction and valence bands. Thus, electrons can be excited from valence band to La doping energy level which provides the photo-generated electrons and holes with UV irradiation. While photo-generated electrons are captured by O_2 molecules to form superoxide radicals, the photo-generated holes are held by H_2O molecules to form hydroxyl radicals. Also, La^{3+} ions act as the electron traps and decrease the electron-hole recombination rate. These trapping prevent electron and hole recombination as they migrate to the catalyst surface [32]. The recombination of electrons and holes excites the 4f electrons of the La, converting the energy corresponding to the 4f→4f transitions into red emission [19].

4. Conclusion

Yttrium vanadate-based powder samples were successfully prepared with solid state reaction method at low sintering temperatures under open atmosphere. Both the undoped/pure and La^{3+}-doped samples show the tetragonal YVO_4 phase. The effect of the La doping was also confirmed by the characterizations. This is because of the similar ionic size of the La^{3+} ($r_{La}{}^{3+}$= 1.172 Å) with the Y^{3+} ion ($r_Y{}^{3+}$= 1.401 Å). Powder samples both exhibits partially agglomerated and the particles are both in irregular shape and size. The EDS profile of both powders also represent the presence of all elements what in each sample must have. The PL studies demonstrate the characteristic emission peaks of undoped YVO_4 has not changed prominently after the introduction of La^{3+} ions while the luminescence intensity varied. The PL emission spectrum of pure YVO_4 has two clear peaks located at 620 and 710 nm in the wavelength range of 600–800 nm which can be related to shallow and deep level trap states and the recombination of electrons and holes at oxygen vacancies in YVO_4, respectively. The major emission peak (at 571 nm) of YVO_4: La^{3+} powder may be assigned to singly ionized oxygen vacancies which became dominated after La^{3+} doping. Moreover, emission bands between 450 and 650 nm were significantly suppressed in YVO_4: La^{3+}. Therefore, La^{3+} doping may modify the intrinsic lattice defects and effectively changes luminescence characteristic with respect to PL characteristics of undoped YVO_4. The effect of La doping on the YVO_4 sample can also be seen from the absorption spectra. With the La doping, there exists an intense band-to-band absorption originated from the contribution of $^1A_1 \rightarrow {}^1T_1$ charge transition around 300 nm overlapped with $^1A_1 \rightarrow {}^1T_2$ charge transition at between 200–350 nm of $VO_4{}^{3-}$ groups. It was seen from the photocatalytic results that lanthanum doping to YVO_4 increased the photocatalytic activity. In addition, energy band gap of the La doped YVO_4 was measured as 3.54 eV which is the sign of the improved photocatalytic performance of the doped YVO_4. The improving in the photocatalytic performance of the doped powders can be attributed to localized energy levels, trapping of the electrons by La^{3+} ions and energy conversion of the 4f electrons of lanthanum. According to the results, La doped YVO_4 is an effective photocatalyst for the water treatment.

Declarations

Ethical Approval

The authors confirm that the present work is unpublished and not under consideration for publication elsewhere.

Competing interests

The authors declare that they have no financial interests or personal relationships that could affect the work.

Authors' contributions

E.K. performed the sample preparation and experimental works. All the authors carried out the analysis, manuscript writing, and did final editing.

Funding

not applicable

Availability of data and materials

not applicable

References

1. S.L. Postel, G.C. Daily, P.R. Ehrlich, Human Appropriation of Renewable Fresh Water, Science, 271 (1996) 785-788.
2. A. Fujishima, K. Honda, Electrochemical Photolysis of Water at a Semiconductor Electrode, Nature, 238 (1972) 37-38.
3. J. Ye, Z. Zou, M. Oshikiri, A. Matsushita, M. Shimoda, M. Imai, T. Shishido, A novel hydrogen-evolving photocatalyst InVO4 active under visible light irradiation, Chemical Physics Letters, 356 (2002) 221-226.
4. S. Kohtani, M. Koshiko, A. Kudo, K. Tokumura, Y. Ishigaki, A. Toriba, K. Hayakawa, R. Nakagaki, Photodegradation of 4-alkylphenols using BiVO4 photocatalyst under irradiation with visible light from a solar simulator, Applied Catalysis B: Environmental, 46 (2003) 573-586.
5. L.Z. Pei, Y.K. Xie, Y.Q. Pei, Y.X. Jiang, H.Y. Yu, Z.Y. Cai, Hydrothermal synthesis of Mn vanadate nanosheets and visible-light photocatalytic performance for the degradation of methyl blue, Materials Research Bulletin, 48 (2013) 2557-2565.
6. X. Zhang, Z. Ai, F. Jia, L. Zhang, X. Fan, Z. Zou, Selective synthesis and visible-light photocatalytic activities of BiVO4 with different crystalline phases, Materials Chemistry and Physics, 103 (2007) 162-167.
7. L. Zhang, H. Fu, C. Zhang, Y. Zhu, Synthesis, characterization, and photocatalytic properties of InVO4 nanoparticles, Journal of Solid State Chemistry, 179 (2006) 804-811.
8. J. Cai, Y. He, X. Wang, L. Zhang, L. Dong, H. Lin, L. Zhao, X. Yi, W. Weng, H. Wan, Photodegradation of RhB over YVO4/g-C3N4 composites under visible light irradiation, RSC Advances, 3 (2013) 20862-20868.
9. Y.K. Kshetri, C. Regmi, H.-S. Kim, S.W. Lee, T.-H. Kim, Microwave hydrothermal synthesis and upconversion properties of Yb3+/Er3+ doped YVO4 nanoparticles, Nanotechnology, 29 (2018) 204004.
10. W. Ryba-Romanowski, YVO4 crystals - puzzles and challenges, Cryst Res Technol, 38 (2003) 225-236.

11. H. Xu, H. Wang, H. Yan, Preparation and photocatalytic properties of YVO4 nanopowders, Journal of Hazardous Materials, 144 (2007) 82-85.
12. Y. Liu, J. Ma, C. Dai, Z. Song, Y. Sun, J. Fang, C. Gao, J. Zhao, Low-Temperature Synthesis of YVO4 Nanoparticles and their Photocatalytic Activity, Journal of the American Ceramic Society, 92 (2009) 2791-2794.
13. L. Yang, G. Li, W. Hu, M. Zhao, L. Sun, J. Zheng, T. Yan, L. Li, Control Over the Crystallinity and Defect Chemistry of YVO4 Nanocrystals for Optimum Photocatalytic Property, European Journal of Inorganic Chemistry, 2011 (2011) 2211-2220.
14. R.M. Mohamed, F.A. Harraz, I.A. Mkhalid, Hydrothermal synthesis of size-controllable Yttrium Orthovanadate (YVO4) nanoparticles and its application in photocatalytic degradation of direct blue dye, Journal of Alloys and Compounds, 532 (2012) 55-60.
15. C.M. Aiube, T.M. Lobo, D. Sousa-Moura, I.B.M. Ferraz, M.E. Osugi, C.K. Grisolia, R. Oliveira, I.T. Weber, Study of YVO4 as a photocatalyst: Correlation between synthetic route and ecotoxicity, Journal of Environmental Chemical Engineering, 6 (2018) 2846-2854.
16. H.J. Zhang, L. Zhu, X.L. Meng, Z.H. Yang, C.Q. Wang, W.T. Yu, Y.T. Chow, M.K. Lu, Thermal and Laser Properties of Nd:YVO4 Crystal, Crystal Research and Technology, 34 (1999) 1011-1016.
17. R.A. Fields, M. Birnbaum, C.L. Fincher, Highly efficient Nd:YVO4 diode-laser end-pumped laser, Applied Physics Letters, 51 (1987) 1885-1886.
18. A.K. Levine, F.C. Palilla, A NEW, HIGHLY EFFICIENT RED-EMITTING CATHODOLUMINESCENT PHOSPHOR (YVO4:Eu) FOR COLOR TELEVISION, Applied Physics Letters, 5 (1964) 118-120.
19. Y. Shiraishi, S. Takeshita, T. Isobe, Two Photoenergy Conversion Modes of YVO4:Eu3+ Nanoparticles: Photoluminescence and Photocatalytic Activity, J. Phys. Chem. C, 119 (2015) 13502-13508.
20. S. Wu, H.-J. Butt, Near-Infrared-Sensitive Materials Based on Upconverting Nanoparticles, Advanced Materials, 28 (2016) 1208-1226.
21. T. Chen, K. Li, H. Mao, Y. Chen, J. Wang, Preparation and Upconversion Emission Investigation of the YVO4: Yb3+/Tb3+/Eu3+ Nanomaterials and Their Coupling with the Au Nanoparticles, Crystal Research and Technology, 55 (2020) 2000001.
22. R. Shannon, Revised effective ionic radii and systematic studies of interatomic distances in halides and chalcogenides, Acta Crystallogr., Sect. A: Found. Crystallogr., 32 (1976) 751-767.
23. M. Duhan, S. Bharadwaj, A. Gupta, H. Kaur, Influence of La doping on structural, photo-luminescence and magnetic properties of SnO2 nanostructures co-doped with Gdk, Mater Lett, 302 (2021).
24. Y.L. Huang, W.L. Zhu, X.Q. Feng, Z.Y. Man, The effects of La3+ doping on luminescence properties of PbWO4 single crystal, J Solid State Chem, 172 (2003) 188-193.
25. Y.X. Liu, G.X. Liu, J.X. Wang, X.T. Dong, W.S. Yu, Reddish-orange-emitting and paramagnetic properties of GdVO4:Sm3+/Eu3+ multifunctional nanomaterials (vol 39, pg 8282, 2015), New J Chem, 39 (2015) 9028-9028.

26. L.S. Yang, S.Y. Peng, M.L. Zhao, L.S. Yu, New synthetic strategies for luminescent YVO4:Ln(3+) (Ln = Pr, Sm, Eu, Tb, Dy, Ho, Er) with mesoporous cell-like nanostructure, Opt Mater Express, 8 (2018) 3805-3819.
27. Y.F. Wang, J. Su, Z.H. Lin, J.C. Zhang, J.J. Chang, Y. Hao, Recent progress on the effects of impurities and defects on the properties of Ga2O3, J Mater Chem C, 10 (2022) 13395-13436.
28. T. Tsuzuki, R.L. He, A. Dodd, M. Saunders, Challenges in Determining the Location of Dopants, to Study the Influence of Metal Doping on the Photocatalytic Activities of ZnO Nanopowders, Nanomaterials-Basel, 9 (2019).
29. Z.Y. Hou, P.P. Yang, C.X. Li, L.L. Wang, H.Z. Lian, Z.W. Quan, J. Lin, Preparation and Luminescence Properties of YVO4:Ln and Y(V, P)O-4:Ln (Ln = Eu3+, Sm3+, Dy3+) Nanofibers and Microbelts by Sol-Gel/Electrospinning Process, Chem Mater, 20 (2008) 6686-6696.
30. M.R. Dolgos, A.M. Paraskos, M.W. Stoltzfus, S.C. Yarnell, P.M. Woodward, The electronic structures of vanadate salts: Cation substitution as a tool for band gap manipulation, Journal of Solid State Chemistry, 182 (2009) 1964-1971.
31. T. Zhang, T. Oyama, A. Aoshima, H. Hidaka, J. Zhao, N. Serpone, Photooxidative N-demethylation of methylene blue in aqueous TiO2 dispersions under UV irradiation, Journal of Photochemistry and Photobiology A: Chemistry, 140 (2001) 163-172.
32. J.B. Kisała, G. Hörner, A. Barylyak, D. Pogocki, Y. Bobitski, Photocatalytic Degradation of 4,4'-Isopropylidenebis(2,6-dibromophenol) on Sulfur-Doped Nano TiO(2), Materials (Basel), 15 (2022).

Figures

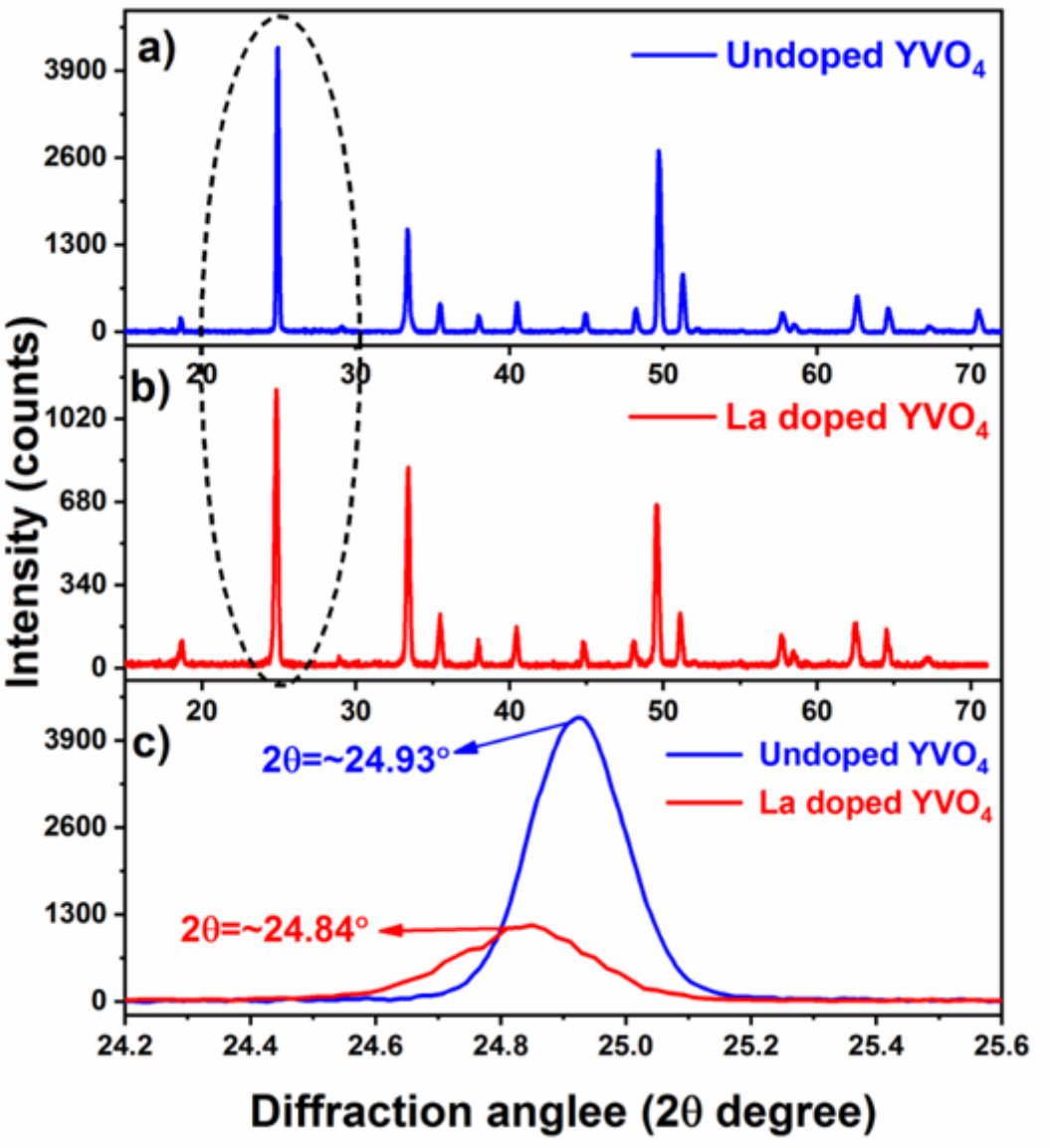

Figure 1

XRD pattern of (a) undoped and (b) La^{3+}-doped YVO_4 powder. (c) The partially enlarged XRD pattern of undoped and doped powders.

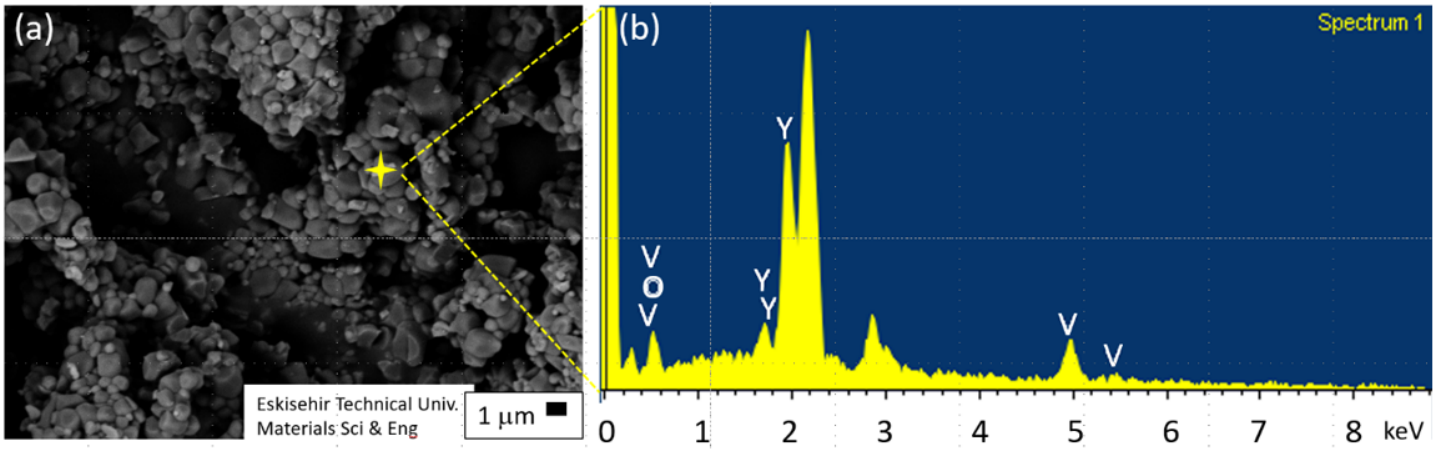

Figure 2

SEM image and EDS profile of undoped YVO_4 powder

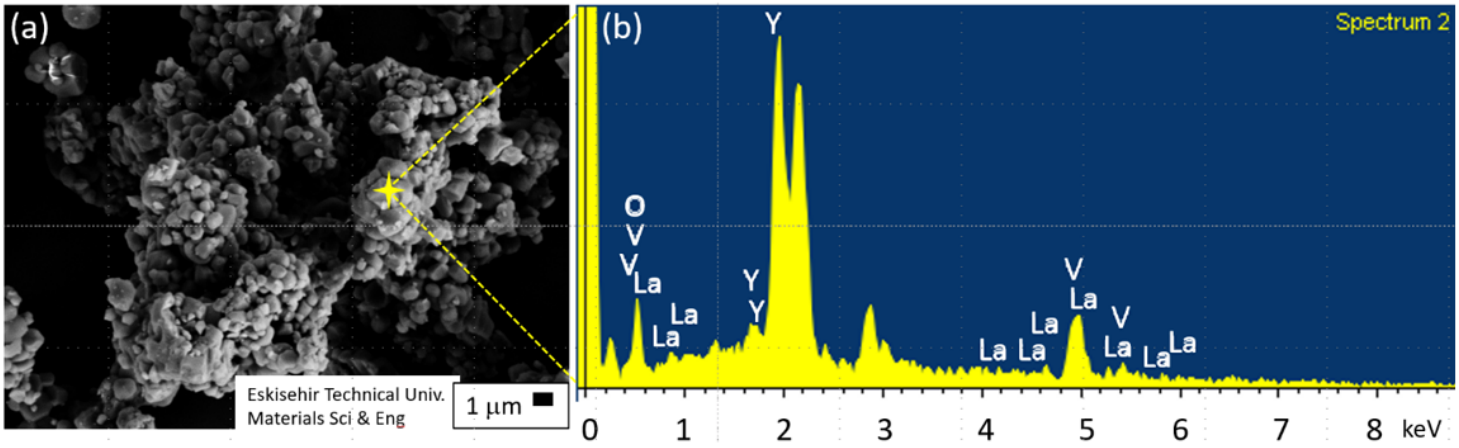

Figure 3

SEM image and EDS profile of La^{3+}-doped YVO_4 powder.

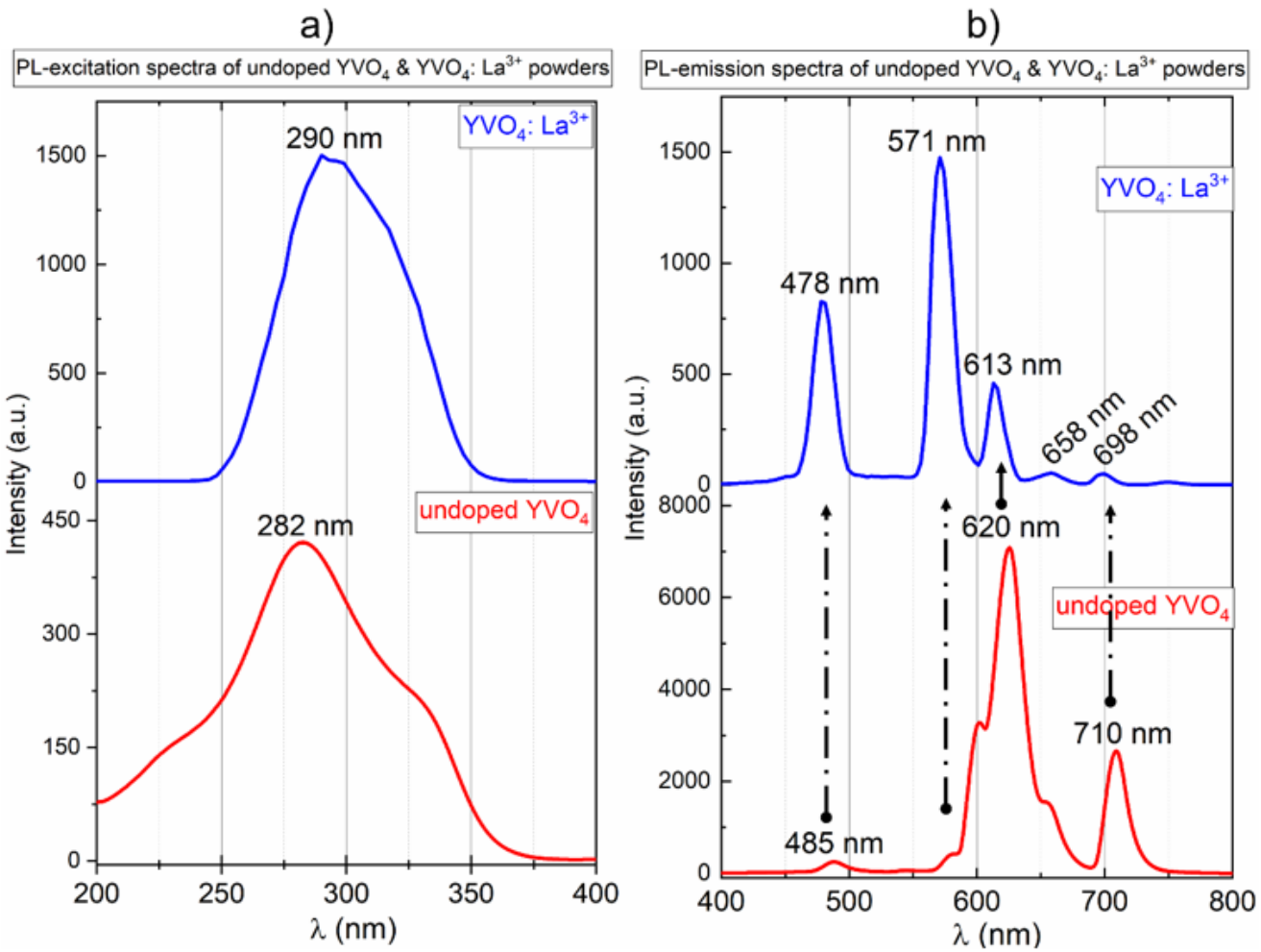

Figure 4

PL excitation and emission spectra of undoped and La^{3+} doped YVO_4 powders.

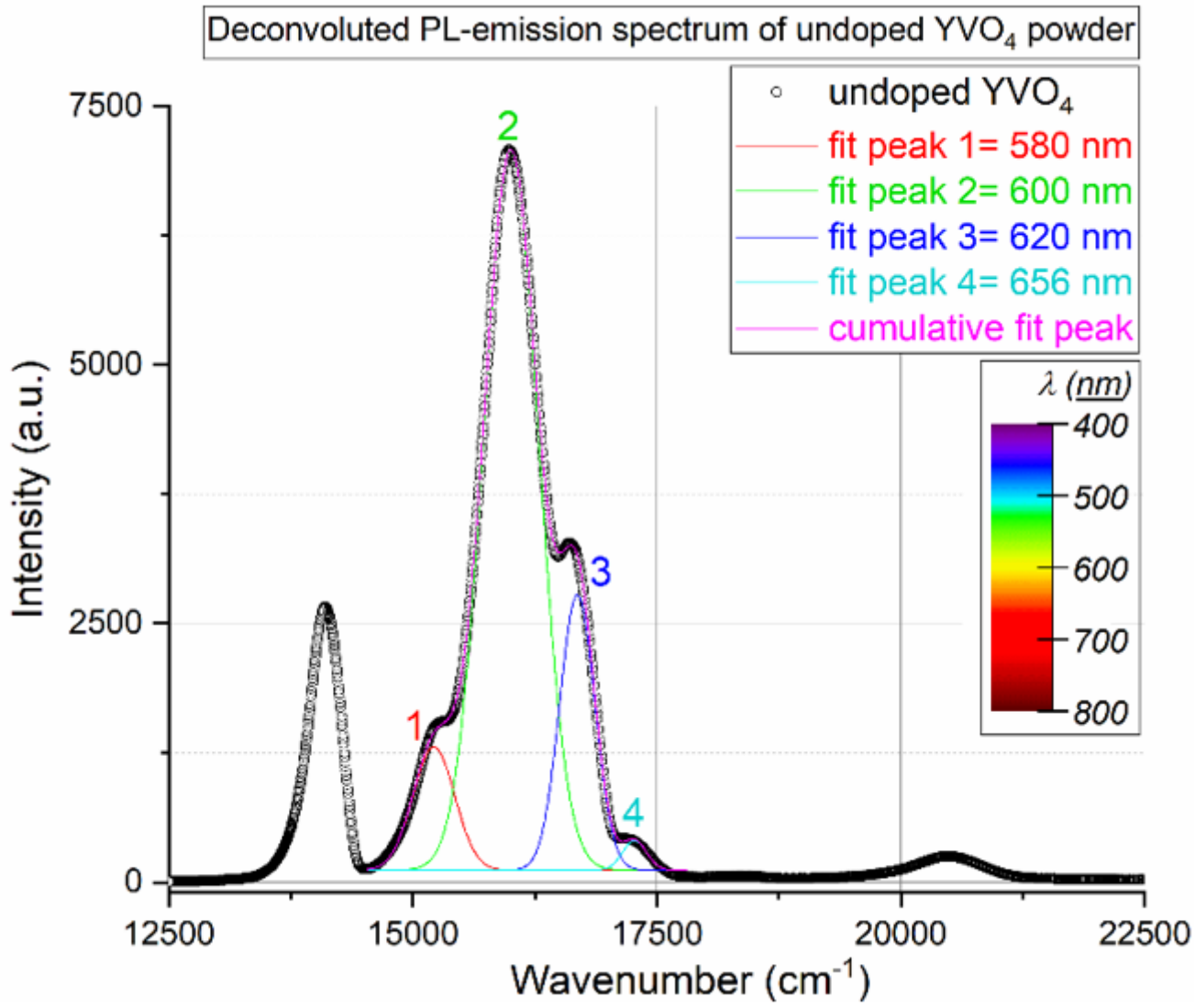

Figure 5

The deconvoluted PL emission spectrum of undoped YVO_4 powder

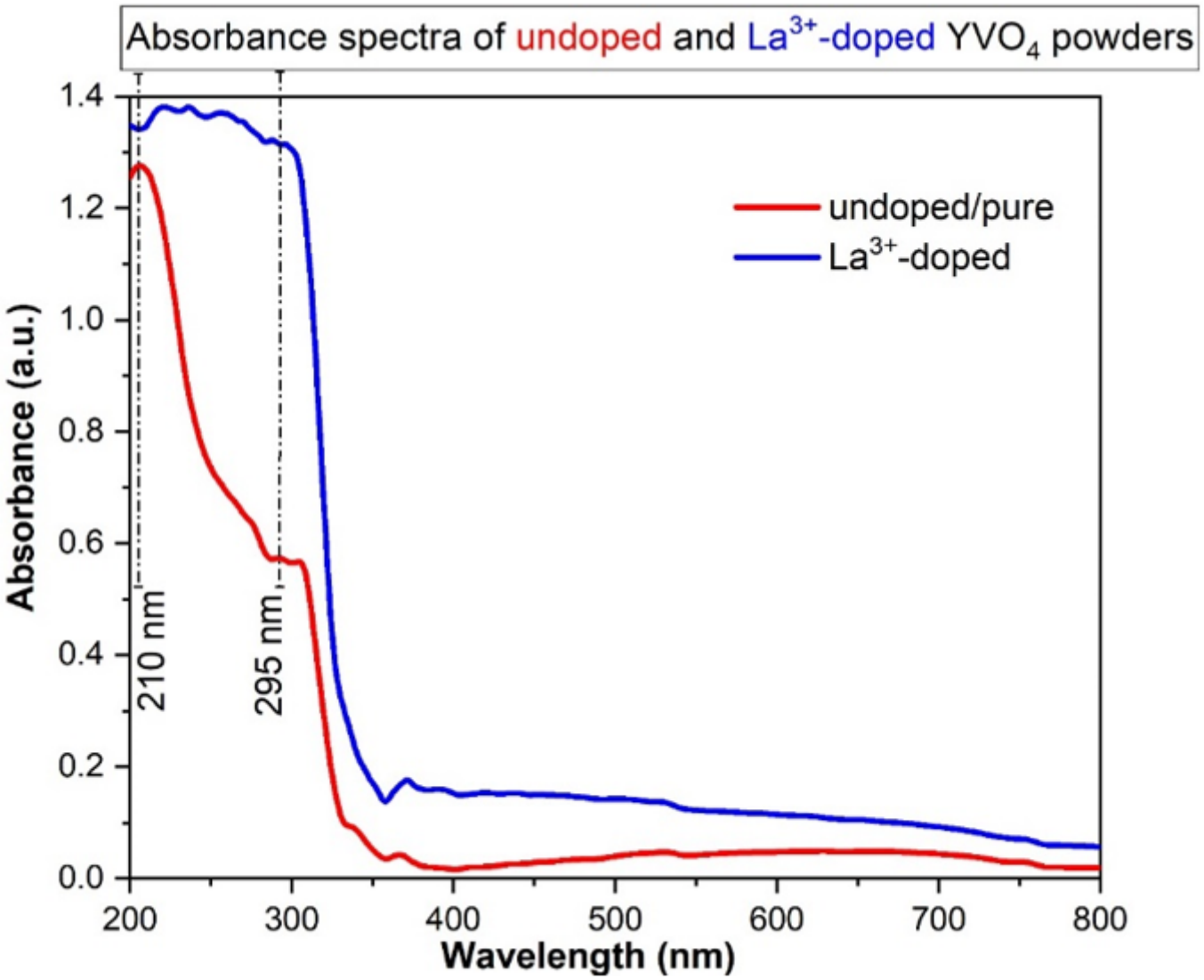

Figure 6

Absorption spectra of undoped/pure YVO_4 and YVO_4: La powders

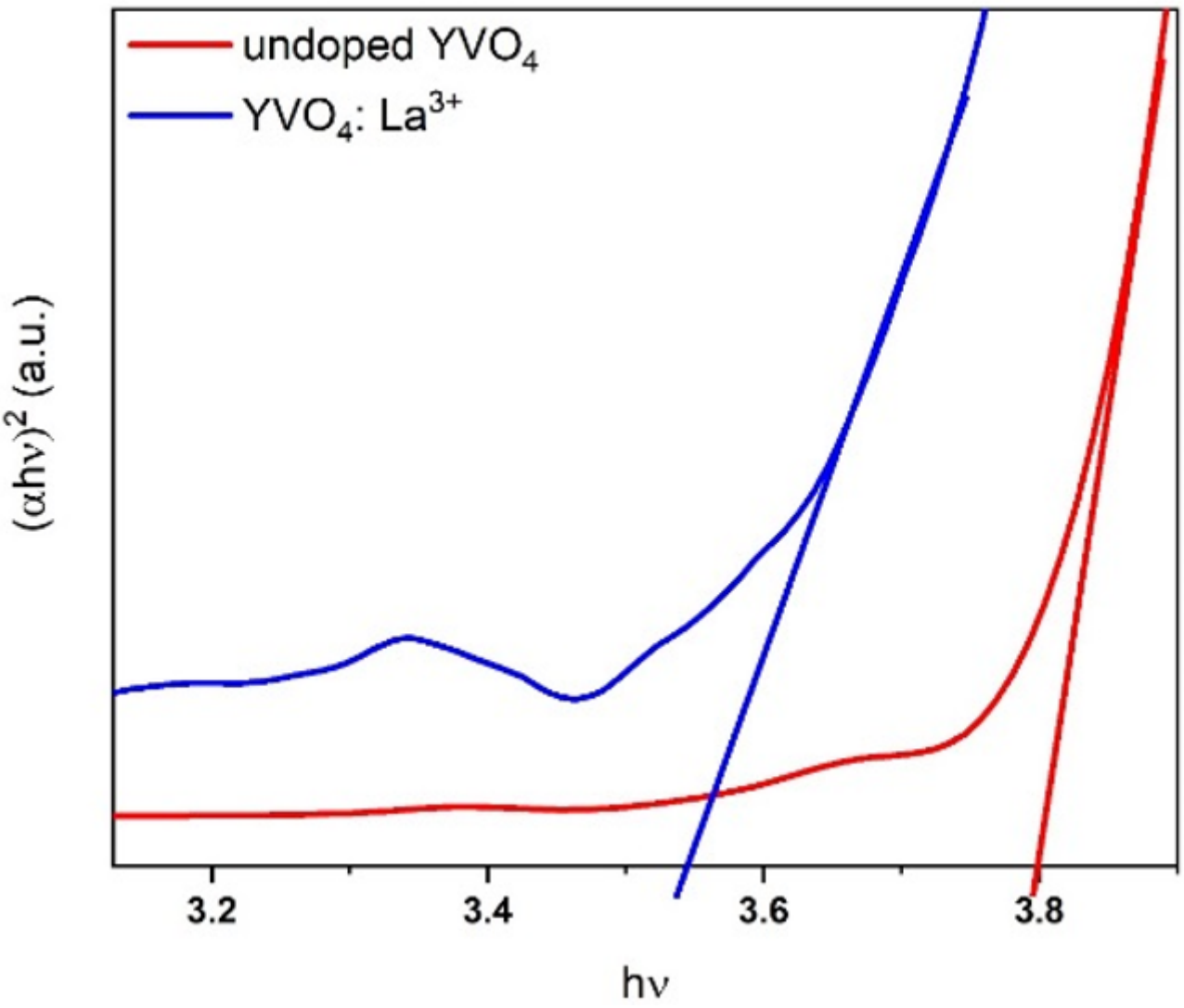

Figure 7

The Tauc plots used to calculate the band gap for undoped and YVO_4: La

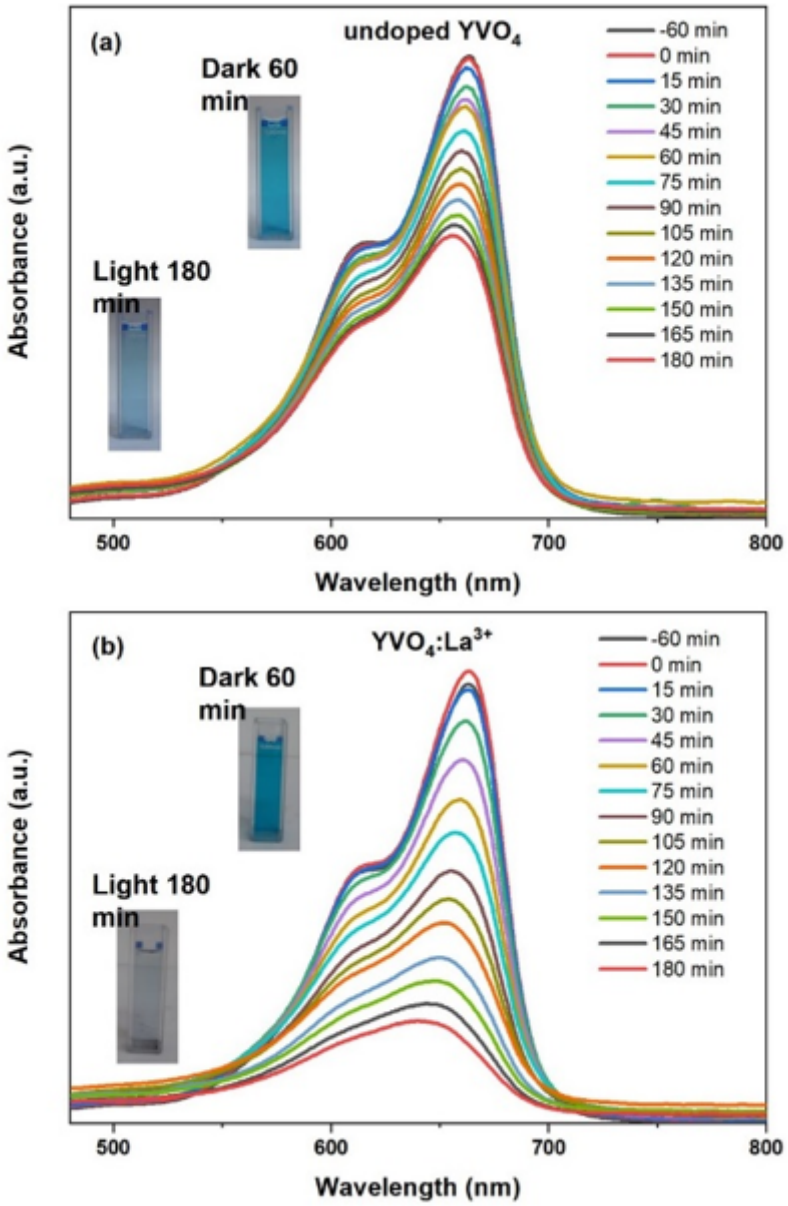

Figure 8

Absorption spectra of MB dye degradation for the undoped YVO_4 and $YVO_4:La^{3+}$ powders under UV light illumination.

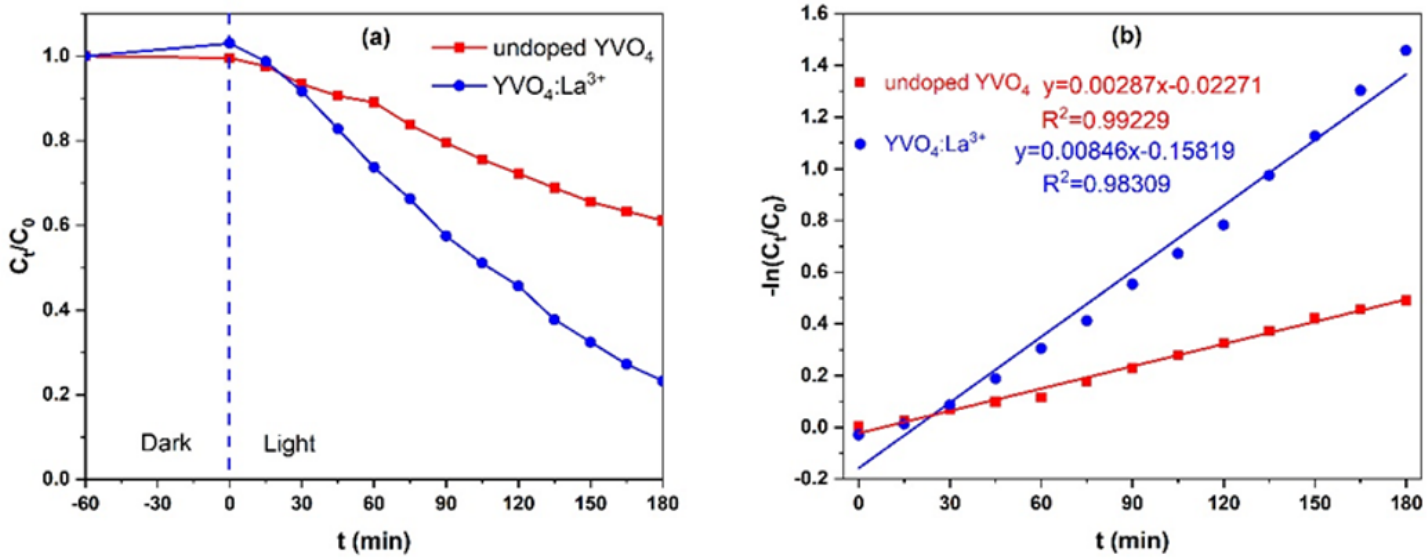

Figure 9

(a) Temporal degradations of MB aqueous solution and (b) kinetic study of the photodegradation for undoped YVO_4 and La^{3+}-doped YVO_4 powders under UV light.

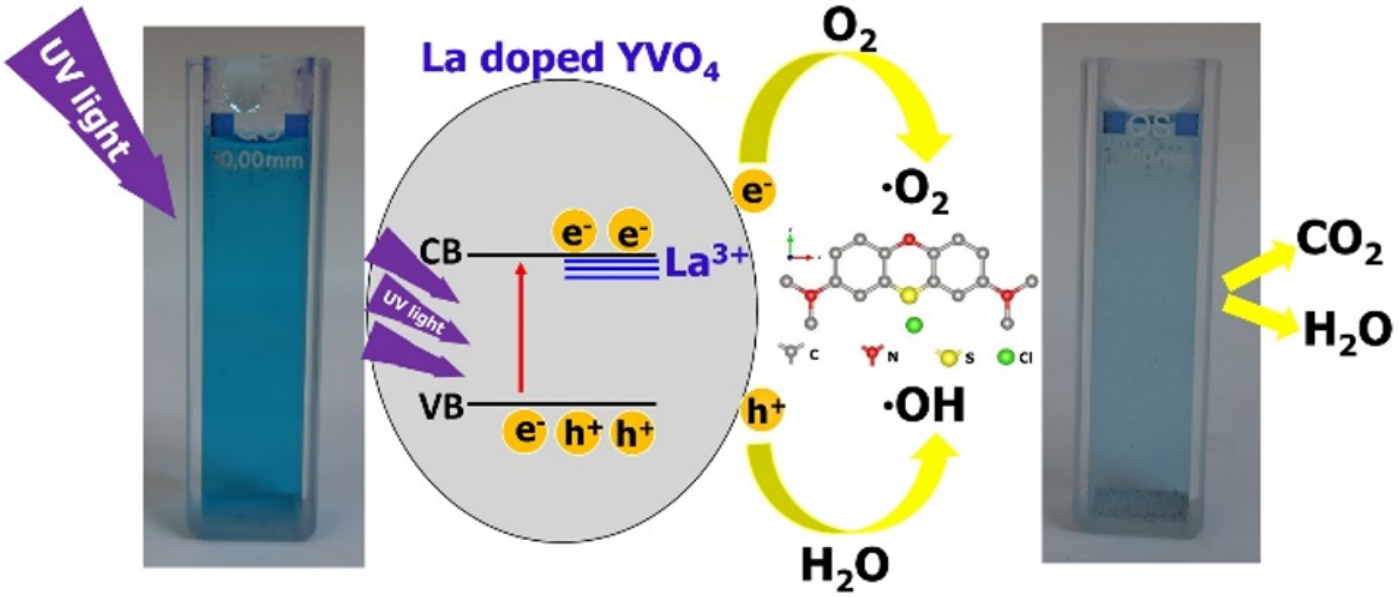

Figure 10

The representative mechanism of photocatalytic activity of La doped YVO_4.